Investigating the effect of distance of carbon steel particles from the impacted surface on mechanical properties in SMAT process of AZ31 using molecular dynamicss

A. Kazemi[1], A. Heidari*[2], K. Amini*[3], F. Aghadavoudi[4], M. Loh-Mousavi[5]

Department of Mechanical Engineering, Khomeinishahr Branch, Islamic Azad University, Khomeinishahr/Isfahan, Iran

Abstract

In the surface mechanical attrition treatment (SMAT) process, the material surface layer is peened with a high-velocity number of carbon steel shot particles. Various parameters such as the distance of the peening gun to the impacted surface can affect the material's surface mechanical properties in the SMAT process. In this paper, the molecular dynamics (MD) approach has been used to study the effect of particle distance from the impacted surface on mechanical and physical behavior of AZ31 after the SMAT process. For this purpose, Universal Force Field (UFF) and Embedded Atom Model (EAM) force field have been utilized for atomic interactions. Based on the molecular simulation results, residual stress, hardness, and temperature of the atomic surface layer have been obtained for various distances. The simulation results demonstrated that reducing the particle distance in the SMAT process increases residual stress and surface layer hardness. Numerically, the maximum residual stress value of 268 MPa has been obtained for a distance of 5 nm in the SMAT molecular simulation results.

Keywords: Molecular Dynamics Approach, Mg-based AZ31 Alloy, SMAT Time, Mechanical Properties.

1. Introduction

Surface Mechanical Attrition Treatment (SMAT) is a novel process that generates nano-crystalline surfaces in metallic alloys [1-3]. The SMAT process can enhance the mechanical properties of the surface layer of metallic materials due to grain refinement [4]. Surface nano-crystallization improves the physical and mechanical properties of the material surface such as hardness, wear resistance, and fatigue properties [5-7].

Numerous studies have been conducted on the factors affecting the mechanical properties of the material in the SMAT process. Duan et al. [8] investigated the nano-crystalline surface layers of AZ31 after the SMAT process. Their results demonstrated that the grain sizes of the AZ31 surface layer have been considerably refined to nanoscale in the SMAT process. Furthermore, SEM images were used to investigate the fracture mechanism of the tensile test of SMAT specimens. Meng et al. [9] studied the microstructure of AZ31 after SMAT. They reported a gradient nanostructure construction and depth-dependent gradient microhardness, from surface to matrix, as a result of the SMAT process. They also observed a significant improvement in the yield strength and ultimate strength of AZ31 Mg alloy after SMAT. Xia et al. [10] reported a gradient nanostructure from the surface layer to the center of AZ31 after the SMAT process. They studied the AZ31 tribological behavior using SEM and dry sliding laboratory tests. The results showed improvement in wear resistance properties after SMAT.

In addition to the experimental methods, numerical methods, such as artificial neural networks or molecular

**Corresponding author*
Email: heidari@iaukhsh.ac.ir
amini@iaukhsh.ac.ir
Address: Department of Mechanical Engineering, Khomeinishahr Branch, Islamic Azad University, Khomeinishahr/Isfahan, Iran
1. PhD Candidate
2. Assistant Professor
3. Associate Professor
4. Assistant Professor
5. Assistant Professor

dynamics (MD) as a new computational method, have presented important results and achievements in predicting the mechanical and physical properties of solids such as alloy-based compounds or nanostructured materials [11-17]. Moradi et al. [14] reported the effects of sphere particle diameter and impact velocity on residual stress and mechanical properties of Ti-6Al-4V as titanium alloy using MD simulation results in the shot peening process. The results showed the residual that the stress values in titanium increased by increasing the particle diameter and velocity. They reported the value of maximum compressive residual stress as -413 MPa at the depth of 10Å from the surface layer. Furthermore, their simulation results showed that the Vickers hardness of titanium is augmented by increasing the size and velocity of the colliding particles at atomic scale. They used two force fields including Lennard-Jones (LJ) and embedded atom method (EAM) for molecular simulation potential functions and compared the obtained results.

In this study, molecular dynamics has been used to investigate the influence of the distance of carbon steel colliding particles from the impacted surface on the mechanical properties of the AZ31 matrix in the SMAT process. Technically, MD simulations in the current study have been conducted in two main steps. At the first step of molecular modeling, the equilibration phase of atomistic structure is performed, and at the second step various physical and mechanical parameters such as surface temperature and residual stress are determined.

2. Molecular Dynamics Method Details

The MD simulation method is one of the computational methods to describe the prediction of material properties at the atomic scale and nanostructures. [15-18]. In this approach, atoms are allowed to interact with each other in various time steps, and the atoms' trajectories are calculated by the numerical solution of Newtonian equations of motion. In this SMAT modeling, spherical particles of carbon steel collide with the surface of AZ31 at a high speed. For molecular modeling of SMAT, initial temperature of atomic structure has been chosen at T_0=300 K. After molecular simulation, various parameters such as residual stress and Vickers hardness were determined and reported at this temperature. In MD simulation, the concept of force field is used to calculate the interaction between atoms [19]. In this study, the atomic interactions between Az31 matrix and carbon steel particle are described using Lennard-Jones (LJ) potential as follows [20]:

$$U(r) = 4\varepsilon\left[\left(\frac{\sigma}{r}\right)^{12} - \left(\frac{\sigma}{r}\right)^{6}\right] \qquad r < r_C \qquad \text{Eq. (1)}$$

$$U(r) = 4\varepsilon\,[(\frac{\sigma}{r_{ij}})^{12} - (\frac{\sigma}{r_{ij}})^{6}] \qquad r \ll r_c$$

where ε is the depth of the potential well and σ is the finite atomic distance at which the potential value reaches to zero. Furthermore, r is the atomic distance between simulated particles in the simulation box. The constant values for Mg, Fe, and C atoms that are used in this molecular simulation are reported in Table 1 [21]. Also, the atomic interactions in two metallic structures including carbon steel particle and AZ31 matrix are defined using Embedded Atom Model (EAM) as presented below [22-23]:

$$E_i = F_a\sum_{i\neq j}\rho_\beta\left(r_{ij}\right) + \frac{1}{2}\sum_{i\neq j}\varphi_{\alpha\beta}\left(r_{ij}\right) \qquad \text{Eq. (2)}$$

Where $\varphi_{\alpha\beta}$ is a pair-wise interaction parameter, ρ_β is the contribution to the charge density from atom j of type β at the coordination of atom I, and F_α is an embedding function that defines the energy required to locate atom i of type α into the charge cloud.

After force-field definitions for atomic structures, Newton's second law Equation is computed as the gradient of atomic force-field [24]:

$$F_i = \sum_{i\neq j}F_{ij} = m_i\frac{d^2r_i}{dt} \qquad \text{Eq. (3)}$$

$$F_{ij} = -\nabla V_{ij} \qquad \text{Eq. (4)}$$

For solving the above equations, the velocity Verlet algorithm was used in the association of motion equations and physical properties of simulated nanostructures calculated in each time step [25-27]. In the velocity Verlet algorithm, the following equations are used to calculate the position and velocity of the particles [25-27]:

$$r\left(t+\Delta t\right) = r\left(t\right) + v\left(t\right)\Delta t + \frac{1}{2}a\left(t\right)\Delta t^2 + O\left(\Delta t^4\right) \qquad \text{Eq. (5)}$$

$$v\left(t+\Delta t\right) = v\left(t\right) + \frac{a\left(t\right)+a\left(t+\Delta t\right)}{2}\Delta t + O\left(\Delta t^2\right) \qquad \text{Eq. (6)}$$

Table 1. The ε and σ constants in LJ potential in the current MD simulations for modeling of atomic interactions between Fe, Mg, and C atoms [21]

Atom type	ε (eV)	σ (Å)
Mg	0.111	3.021
Fe	0.013	2.912
C	0.105	3.851

The schematic of molecular structures is shown in figure 1. In this figure, the AZ31 atoms are placed in a rectangular box, and the colliding carbon steel particles are placed in a spherical atomic mass at the top of the AZ31 atom box at a certain distance. Periodic boundary conditions are considered for the simulation box in the X and Y directions and fixed conditions in the Z direction [28]. The spherical atomic structure of carbon steel has a diameter of 1 nm. The equilibration of the simulation box has been done using a Nose-Hoover thermostat with the time step of Δt=1 fs [29-30].

3. Results and Discussion

3.1. Equilibration Phase Outputs

The equilibration phase of the atomic structures of AZ31 matrix and carbon steel particle at the initial condition (T=300K) was performed for 10000000 time steps. The results in this step indicated that the atoms coordination in AZ31 and carbon steel particle were appropriately adopted to the UFF and EAM force fields. Numerically, the physical stability of the atomic structure is described by total energy and temperature calculation. Figure 2 shows the variation of the total energy of the atomic model as a function of the time step in the molecular dynamics calculations at the equilibration phase. This figure shows that the system's total energy has been converted into a finite value after 10 ns. This result indicates the reduction of atoms' oscillation amplitude and consequently the physical stability was detected for the atomic simulation box. Numerically, the temperature of AZ31 matrix-carbon steel particle reaches 300 K after 1000000 time steps.

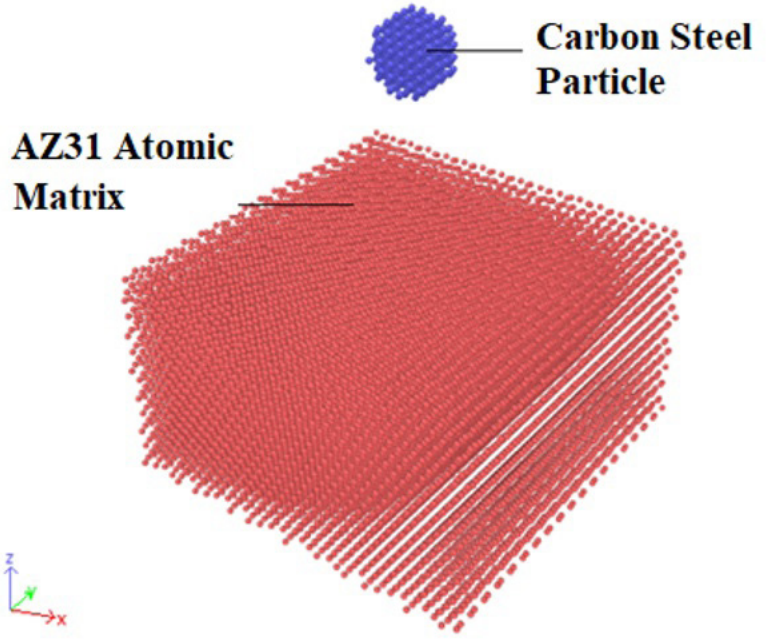

Fig. 1. Schematic of atomic arrangement of carbon steel atom and AZ31 matrix in atomic simulation of the SMAT process.

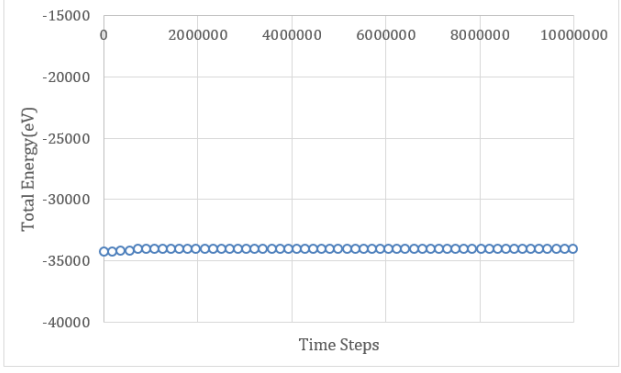

Fig. 2. The total energy of the atomic matrix- particle as a function of computational time steps.

3.2. Residual Stresses

After the equilibrium phase of simulated atomic structures, the carbon steel particle was accelerated toward the AZ31 matrix to create the conditions of the SMAT process in atomistic modeling. The distance of the peening gun to the impacted surface or distance of the colliding carbon steel atomic structure from surface AZ31 matrix, which is defined in this paper as the SMAT height, is an important parameter in this mechanical procedure. In this study, to investigate the effects of the SMAT height variation, the range of SMAT height between 5nm and 30nm is considered. The SMAT process causes plastic deformation and residual stress on the surface of the matrix. Physically, this parameter indicates the force intensity implemented to the pristine matrix. As reported in Figure 3, the residual stress decreased as the SMAT height increased. So, it is expected that by increasing the SMAT height, the atomic position evolution would decrease and less new crystal regions be detected in the AZ31 matrix. Numerically, as the SMAT height changes from 5nm to 30 nm, the residual stress decreases from 268 MPa to 255 MPa. Considering both the simulation results of molecular dynamics and the fact that the presence of residual stress reduces the probability of crack growth and increases fatigue resistance, decreasing the SMAT height to the minimum possible allows more residual stresses.

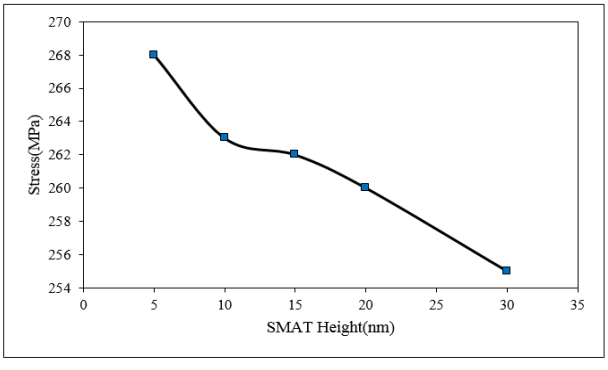

Fig. 3. The maximum residual stress of the AZ31 matrix as a funcion of the SMAT height.

3.3. Surface Temperature

The carbon steel particle colliding with the pristine AZ31 matrix increases the atomic fluctuations in the surface of the metallic matrix. Consequently, the mobility of Mg atoms in the surface regions increases. Computationally, as the atomic mobility or velocity increases, the temperature of the atomic structure changes based on the following equation:

$$\frac{1}{2}mv^2 = \frac{3}{2}kT \qquad \text{Eq. (7)}$$

where k is the Boltezman constant. Figure 4 shows the variations of AZ31 surface temperature as the SMAT height changes in the range of 5 to 30 nm. The MD outputs of figure 4 indicated that as the SMAT process height increases the surface temperature decreases. So it is concluded that as the SMAT height increases, the amplitude of atomic fluctuations decreases, and this procedure causes surface temperature decreasing in the simulated samples. Numerically, by the SMAT height increasing from 5 nm to 30 nm, surface temperature changes from 345 K to 330 K, respectively.

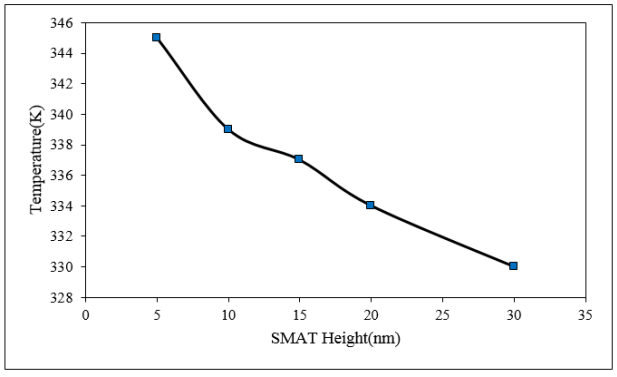

Fig. 4. The surface temperature variations as a function of the AZ31 SMAT height.

3.4. Hardness

Historically, the Vickers hardness test was introduced in 1921 as a new method to measure the hardness of alloy-based materials. Technically, this test is usually easier to use than other hardness tests because the hardness calculations in this method are independent of the size of the indenter. The SMAT process increases the surface hardness of the AZ31 matrix. The amount of hardness can be calculated based on the Vickers equation through the results of molecular dynamics simulation. As can be seen in figure 5, the percentage increase in hardness decreases with increasing the height.

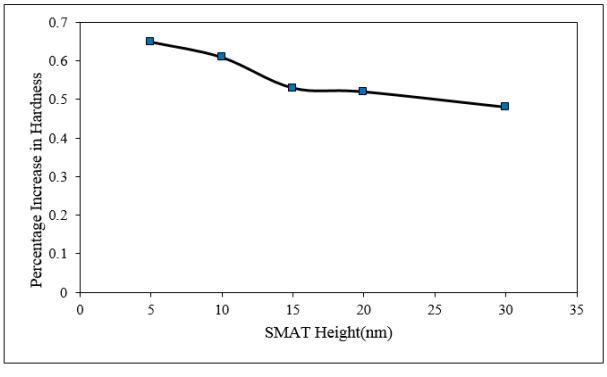

Fig. 5. The percentage increase in hardness of AZ31 as a function of the SMAT height.

3.5. The Atomic Matrix Wear after the SMAT Process

The SMAT process in simulated structures causes the departure of surface atoms from the pristine sample. The number of departed Mg atoms from the AZ31 matrix after the SMAT test in the current computational study has been assumed as the wear inside the MD simulation box. Figure 6 shows the number of departed atoms as a function of the SMAT height. From the MD results in this section it is concluded that height increases cause the attraction force to increase between various surface atoms. With this type of force increasing, the stability of atoms in this region enlarged and fewer atoms departed from the AZ31 structure. Figure 6 shows as the height increased to 30 nm, the number of departed atoms from the simulation box reached 31 atoms.

3. 6. Roughness of Atomic Matrix

In the final step of the current study, the roughness of the AZ31 sample after the SMAT process was investigated using molecular simulation results. To describe the roughness of the simulated structure with the LAMMPS package, the order parameter of the atomic model was calculated. Computationally, this parameter changes between 0 and 1 value. Figure 7 indicates that the SMAT height increasing causes an increase in the order parameter of the pristine alloy. The MD outputs in this section show that atomic evolution in the AZ31 sample decreases by the SMAT height enlarging and less mechanical properties improvement occurs in this structure.

4. Conclusions

In the current computational study, the molecular dynamics (MD) approach has been used to simulate the surface mechanical attrition treatment (SMAT) process in the AZ31 matrix with carbon steel particles. The computational study was done in two main steps. Firstly, the equilibrium phase of atomic compounds at 300 K was performed at the initial temperature. After equilibrium phase detection, the SMAT process simulation with various heights was done and the following results were obtained:

- As the SMAT process height increases, the maximum ratio of residual stress reaches to 268 MPa.
- The surface temperature decreased as the AZ31 SMAT process height increased.
- The percentage of hardness increase of AZ31 matrix reached 0.74 value by the SMAT height.
- By the SMAT process height increase to 30 nm the number of departed atoms from the surface of the AZ31 structure decreases to 31 atoms.
- The order parameter of the alloy matrix is affected by the SMAT process height. Numerically, the order parameter value reaches 0.12 in the SMAT height simulation.

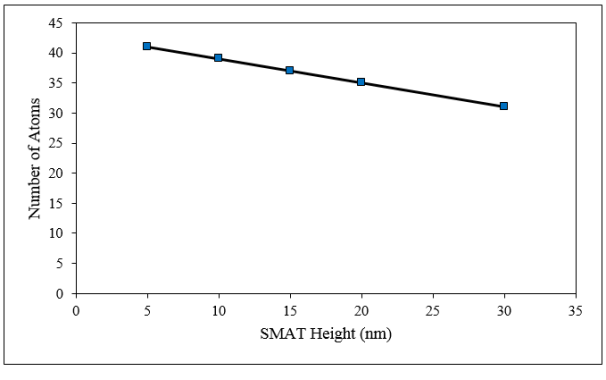

Fig. 6. The number of departed atoms from AZ31 matrix as a function of the SMAT height.

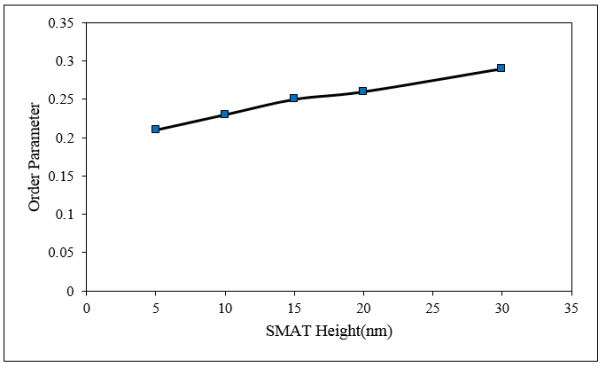

Fig. 7. The order parameter of the AZ31 sample as a function of SMAT height.

References

1. K. Lu, J. Lu, Nanostructured surface layer on metallic materials induced by surface mechanical attrition treatment, Mater. Sci. Eng. A 375 (377) (2004) 38–45.
2. N. Tao, H. Zhang, J. Lu, K. Lu, Development of nanostructures in metallic materials with low stacking fault energies during surface mechanical attrition treatment (SMAT), Mater. Trans. 44 (10) (2003) 1919–1925.
3. T. Roland, D. Retraint, K. Lu, J. Lu, Enhanced mechanical behavior of a nanocrystallised stainless steel and its thermal stability, Mater. Sci. Eng. A 445 (446) (2007) 281–288.
4. T. Roland, D. Retraint, K. Lu, J. Lu, Fatigue life improvement through surface nanostructuring of stainless steel by means of surface mechanical attrition treatment, Scr. Mater. 54 (11) (2006) 1949–1954.
5. L. Waltz, D. Retraint, A. Roos, C. Garnier, P. Olier, Effect of interfacial oxidation occurring during the duplex process combining surface nanocrystallisation and corolling, Surf. Coat. Technol. 205 (19) (2011) 4608–4613.
6. M. Chemkhi, D. Retraint, A. Roos, C. Demangel, Role and effect of mechanical polishing on the enhancement of the duplex mechanical attrition/plasma nitriding treatment of AISI 316L steel, Surf. Coat. Technol. 325 (2017) 454–461.
7. L. Wen, Y. Wang, Y. Zhou, L.X. Guo, J.H. Ouyang, Iron-rich layer introduced by SMAT and its effect on corrosion resistance and wear behavior of 2024 Al alloy, Mater. Chem. Phys. 126 (1–2) (2011) 301–309.
8. M. Duan, L. Luo, Y. Liu, Microstructural evolution of AZ31 Mg alloy with surface mechanical attrition treatment: Grain and texture gradient, J. Alloys. Compd. 823 (2020)153691.
9. X. Meng, M. Duan, L. Luo, D. Zhan, B. Jin, Y. Jin, J. Lu, The deformation behavior of AZ31 Mg alloy with surface mechanical attrition treatment, Mater. Sci. Eng. A. 707 (2017) 636–646.
10. S. Xia, Y. Liu, D. Fu, B. Jin, J. Lu, Effect of Surface Mechanical Attrition Treatment on Tribological Behavior of the AZ31 Alloy, J. Mater. Sci.Tech. 32 (12) (2016) 1245–1252.
11. M. Mahmoodi, H. Tagimalek, H. Sohrabi, M.R. Maraki, Using the artificial neural network to investigate the effect of parameters in square cup deep drawing of aluminum-steel laminated sheets, I.J.I.S.S.I. 17(2) (2020) 1-3.
12. S. A. Eftekhari, D. Toghraie, M. Hekmatifar, R. Sabetvand, Mechanical and thermal stability of armchair and zig-zag carbon sheets using classical MD simulation with Tersoff potential. Phys. E: Low- Dimens. Syst. Nanostructures.133 (2021) 114789.
13. L. Zhao, M.K.M. Nasution, M. Hekmatifar, The improvement of mechanical properties of conventional concretes using carbon nanoparticles using molecular dynamics simulation, Sci. Rep. 11(2021) 20265.
14. A. Moradi, A. Heidari, K. Amini, F. Aghadavoudi, R. Abedinzadeh, Molecular modeling of Ti-6Al-4V alloy shot peening: the effects of diameter and velocity of shot particles and force field on mechanical properties and residual stress, Simul. Mater. Sci. Eng. 29(6) (2021) 065001.
15. D. T. Semiromi, A. R. Azimian, Molecular dynamics simulation of nonodroplets with the modified Lennard-Jones potential function, Heat. Mass. transfer. 47(5) (2011) 579-588.
16. H. Noorian, D. Toghraie, A. R. Azimian, The effects of surface roughness geometry of flow undergoing Poiseuille flow by molecular dynamics simulation, Heat. Mass. Transfer. 50(1) (2014) 95-104.
17. D. T. Semiromi, A. R. Azimian, Nanoscale Poiseuille flow and effects of modified Lennard–Jones potential function, Heat. Mass. Transfer. 46(7) (2010) 791-801.
18. D. T. Semironi, A. R. Azimian, Molecular dynamics simulation of liquid–vapor phase equilibrium by using the modified Lennard-Jones potential function, Heat. Mass. Transfer. 46(3) (2010) 287-294.
19. M. Griebel, S. Knapek, G. Zumbusch, Numerical Simulation in Molecular Dynamics, Ber. Hei. Spr. (2007) 17-36.
20. J. E. Jones "On the determination of molecular fields. —II. From the equation of state of a gas", S. A. Cont. Pap. Math. Phys. Char. 106 (738) (1924) 463–477.
21. A. K. Rappe, C. J. Casewit, K. S. Colwell, W. A. Goddard, W. M. Skiff, UFF, a full periodic table force field for molecular mechanics and molecular dynamics simulations, J. A. C.S. 114(25) (1992) 10024–10035.
22. M. S. Daw, B. Mike, "Embedded-atom method: Derivation and application to impurities, surfaces, and other defects in metals", Phys. Rev. B. 29 (12) (1984) 6443–6453.
23. M. S. Daw, S. M. Foiles, M. I. Baskes, The embedded-atom method: a review of theory and applications, Mat. Sci. Eng. Rep. 9 (7–8) (1993) 251.
24. T. Schlick, Molecular modeling and simulation: an interdisciplinary guide, New York, Springer, (2010).
25. L. Verlet, Computer "Experiments" on Classical Fluids. I. Thermodynamical Properties of Lennard−Jones Molecules, Phys. Rev. 159 (1) (1967) 98–103.
26. W. H. Press, S. A. Teukolsky, W. T. Vetterling, B. P. Flannery, Section 17.4. Second-Order Conservative Equations". Numerical Recipes: The Art of Scientific computing (3rd ed), New York, Cambridge University Press, (2007).
27. E. Hairer, C. Lubich, G. Wanner, Geometric numerical integration illustrated by the Störmer/Verlet method, Acta. Numerica. 12 (2003) 399–450.
28. W. Mai, P. Li, H. Bao, X. Li, L. Jiang, J. Hu, D. H. Werner, Prism-Based DGTD With a Simplified Periodic Boundary Condition to Analyze FSS With D2n Symmetry in a Rectangular Array Under Normal Incidence, IEEE. Antennas. Wirel. Propag. Lett.18(4) (2019) 771–775.

29. S. Nosé, A unified formulation of the constant temperature molecular-dynamics methods, J. C. Phys. 81 (1) (1984) 511–519.

30. W. G. Hoover, Canonical dynamics: Equilibrium phase-space distributions, Phys. Rev. A. 31 (3) (1985) 1695–1697.